LECTURE 2:
ELECTRON EMISSION AND CATHODE EMITTANCE

DAVID H. DOWELL
STANFORD LINEAR ACCELERATOR CENTER

Abstract. The objectives of this lecture are to define the basic electron emission statistics, describe the electrical potentials at the cathode surface, define the thermal emittance and derive the cathode emittance for thermal, photoelectric and field emission.

1. Introduction

The electron density inside a cathode is many orders of magnitude higher than that of the emitted electron beam. This is seen by considering that the density of conduction band electrons for metals is 10^{22} to 10^{23} electrons/cm^3, roughly one electron per atom. Whereas the density of electrons in a 6 ps long, 200 micron diameter cylindrical bunch with 1 nC of charge is 1.1×10^{14} electrons/cm^3. Thus the transition from bound to free reduces the electron density by eight to nine orders of magnitude. In addition, the energy spread, or thermal energy of the electrons inside the cathode material is low. For example, in copper the energy spread near the Fermi energy is k_BT or 0.02 eV at room temperature (300 degK). However, in order to release these cold, bound electrons, one needs to heat the cathode to approximately 2500 degK, resulting in a beam with a thermal energy of 0.20 eV.

In general, the electron temperature of the emission process determines the fundamental lower limit of the beam emittance. This ultimate emittance is often called the thermal emittance, due to the Maxwell-Boltzmann (MB) distribution of thermionic emitters. Strictly speaking, the term 'thermal emittance' applies only to thermionic emission, but the concept of thermal emittance or the intrinsic cathode emittance can be applied to all three fundamental emission processes:

1. thermionic emission,
2. photo-electric emission and
3. field emission.

This lecture begins with definitions of Maxwell-Boltzmann and Fermi-Dirac statistics, and discusses the electric fields at the cathode surface which the electron needs to overcome to escape. Then the physics of each of the three emission processes is described and their cathode emittances are derived.

2. Electron Statistics and the Emission Processes

Elementary particles in general can be classified as either bosons or fermions depending upon whether they have integer or half integer spin, respectively. Bosons obey classical Maxwell-Boltzmann statistics, while fermions follow Dirac-Fermi statistics. These statistics define the probability a particle occupies an given energy

state based on the the distribution of N-particles on k-energy intervals for the two particle types:

1. particles any number of which can share the same energy state, follow the Maxwell-Boltzmann distribution.

2. particles which cannot share the same energy state having only one particle per energy state, follow Fermi-Dirac distribution.

The first particle type obeys classical Maxwell-Boltzmann (M-B) statistics with the energy distribution of occupied states given by,

$$f_{MB} = e^{-E/k_B T} \tag{1}$$

For the second particle type, of which electrons are are a member being fermions, the energy distribution of occupied states (DOS) is given by the Fermi-Dirac (F-D) function,

$$f_{FD} = \frac{1}{1 + e^{(E-E_F)/k_B T}} \tag{2}$$

The distributions are compared in Figure 1, showing they have very nearly the same high energy tails. During thermionic emission the cathode is heated to high temperature to increase the high energy tail of the distribution and promote emission. In this case, M-B statistics is completely valid and the classical concept of temperature applies. However, as will be shown, photo-electric and field emission involves the excitation of electrons from below the Fermi energy and not only the tail of the distribution. In these cases, F-D statistics should be used.

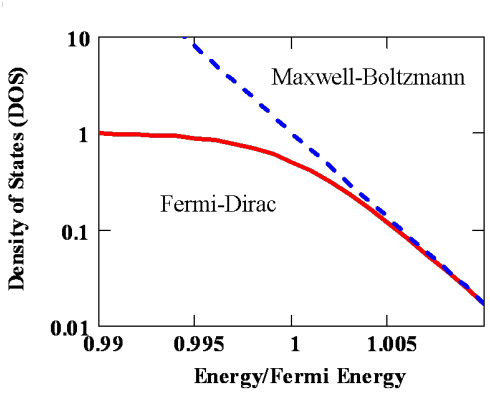

FIGURE 1. Comparison of the particle energy distributions in the high-energy tails of the classical Maxwell-Boltzmann and the quantum mechanical Fermi-Dirac functions.

In some applications electrons are produced using two of more of these three processes. A good example is field emission, which is usually considered to occur at low temperature, but in practice is often combined with thermionic emission in the high field of thermionic RF guns. And there are proposals for using all three processes as in photo-assisted thermionic cathodes for high-field RF guns.

3. Fields Near the Cathode Surface

An important aspect of electron emission concerns the fields and potentials at and extremely near the cathode surface, and how these fields affect the electron

states. The electric potential energy as a function of distance from the cathode is given by

$$e\Phi = e\phi_{work} - \frac{e^2}{16\pi\epsilon_0 x} - eE_0 x \tag{3}$$

which is the sum of the work function, ϕ_{work}, the image charge potential and the applied electric field, E_0.

Comparison of the electric fields and the energy density of occupied states near a metal-vacuum boundary is shown in Figure 2. The total external potential, Φ, is the sum of applied and image fields for a single electron, and peaks approximately 2 nm from the surface. Electrons can escape with energies greater than the work function or those with lower energy can tunnel through the barrier. In the cases of thermionic and photo-emission, the escaping electrons must have energies greater than the barrier. In field emission, electrons tunnel through the barrier. This is an important distinction: In the first two the electrons are excited above the barrier to escape, while in field emission the barrier height is lowered by an external field to encourage tunneling.

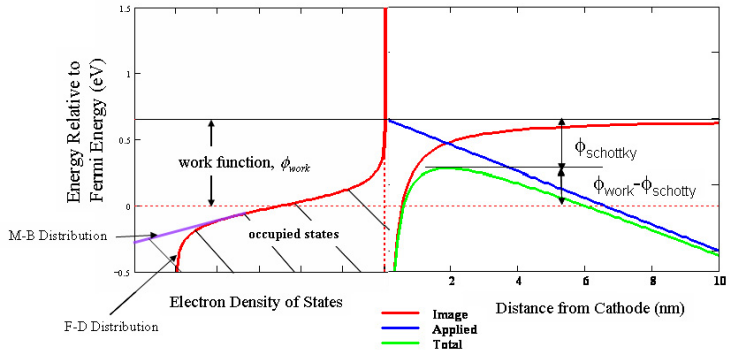

FIGURE 2. The potential energy barrier near the cathode surface (right) and the density of occupied states (left) are plotted within 10 nm of a metallic surface. The work function barrier is produced by an excess of electrons spilling out from inside the cathode to a distance of less than an angstrom. The image potential is for a single electron and the applied field corresponds to 100 V/micron.

The temperature of the electron gas in the bulk material affects the probability of emission and the emitted electron energy distributions for all three phenomena. The reduction of the barrier by the applied field is called the Schottky effect and plays a central role in all emission processes, especially field emission. Photo-electric emission promotes electrons directly from the energy region near the Fermi energy. In the following sections, the underlying physics for these three processes will be described.

4. Thermionic Emission

In order for an electron to escape a metal it needs to have sufficient kinetic in the direction of the barrier to overcome the work function,

$$\frac{mv_x^2}{2} > e\phi_{work} \Rightarrow v_x > \sqrt{\frac{2e\phi_{work}}{m}} \tag{4}$$

Assume that the cathode has an applied electric field large enough to remove all electrons from the surface, so there is no space charge limit for emission, but still low enough as to not affect the barrier height. Then the thermionic current density for a cathode at temperature $T$is given by,

$$j_{thermionic} = n_0 e\langle v_x\rangle = n_0 e\int_{v_x>\sqrt{\frac{2e\phi_{work}}{m}}} v_x f_{FD} d\vec{v} \tag{5}$$

The region of integration over the F-D distribution is shown in Figure 3.

As discussed above, the interactions involving the high energy electrons in the tail of the Fermi-Dirac density of states (The F-D distribution is essentially identical to the classical M-B for energies greater than $1.005E_F$, as shown in Figure 1.), allows it's replacement with the classical, Maxwell-Boltzmann distribution,

$$f_{MB} = e^{-E/k_BT} \tag{6}$$

The equation for the current density is then,

(7)

$$j_{thermionic} = n_0 e\int_{v_x>\sqrt{\frac{2e\phi_{work}}{m}}} v_x f_{MB} d\vec{v} = n_0 e\int_{v_x>\sqrt{2e\phi_{work}/m}} v_x e^{-\frac{m(v_x^2+v_y^2+v_z^2)}{2k_BT}} d\vec{v}$$

Performing these simple integrals gives the thermionic current density,

$$j_{thermionic} = 2n_0 e\left(\frac{2k_BT}{m}\right)^2 e^{-\phi_{work}/k_BT} \tag{8}$$

Or regrouping the leading constants, gives the Richardson-Dushman (R-D) equation for thermionic emission [Reiser, p 8],

$$j_{thermionic} = A(1-r)T^2 e^{-\phi_{work}/k_BT} \tag{9}$$

Here A is 120 $amp/cm^2/degK^2$, and (1-r) accounts for the reflection of electrons at the metal surface. The reflection and refraction of electrons as they transit the surface is discussed in a later section. In terms of fundamental quantities, the universal constant A is ["Solid State Physics", by Ashcroft and Mermin, p. 363]

$$A = -\frac{em}{2\pi^2\hbar^3} \tag{10}$$

The exponential dependence upon temperature of the R-D equation illustrates how thermionic current rises rapidly with temperature, and with decreasing work function. This same work function applies to photo-electric and field emission only for metals. In semi-conductors the thermionic work function is the same as metals, but the threshold for photoelectric emission is Ef + Egap/2 +EA.

The velocity distribution for thermally emitted electrons is obtained from the derivative of Maxwell-Boltzmann particle distribution,

$$\frac{1}{n_e}\frac{dn(v_x)}{dv_x} = \frac{m}{k_BT} v_x e^{\frac{-mv_x^2}{2k_BT}} \tag{11}$$

Figure 4 shows the energy distribution assuming the emitted electrons obey Maxwell-

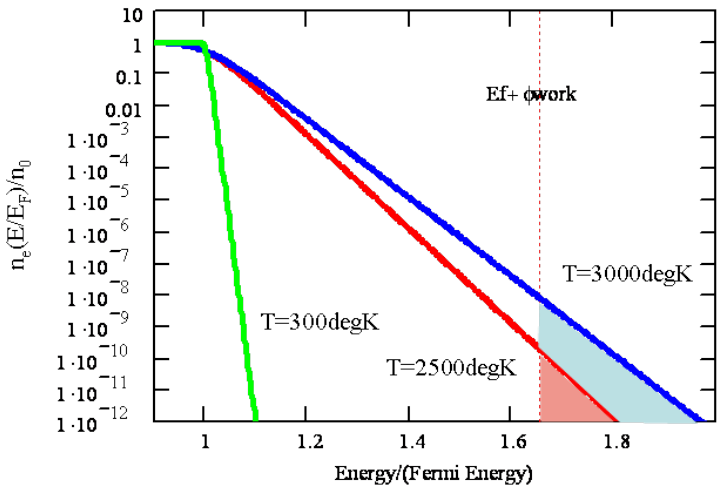

FIGURE 3. Fermi-Dirac energy distributions for thermionic emission. Electrons in the high energy tail of the distribution (energies greater than the work function) are thermally emitted for cathode temperatures of 2500 (red-pink) and 3000 (blue-aqua) degK.

Boltzmann statistics. At room temperature, the mean transverse velocity is 9×10^4 m/s, or 0.025 eV. The initial spread in transverse velocity due to the electron temperature gives the beam angular divergence and hence its thermionic emittance.

Following Lawson[Lawson,p. 209], we assume the normalized emittance is evaluated close to the cathode surface where the electron flow is still laminar (no crossing of trajectories) and any correlation between position and angle can be ignored. In this case, normalized cathode emittance is given by,

$$\epsilon_N = \beta\gamma\sigma_x\sigma_{x'} \tag{12}$$

The root-mean-square (rms) beam size, σ_x, is given by the transverse beam distribution which for a uniform radial distribution with radius R_c is $R_c/2$. The rms divergence is given by

$$\sigma_{x'} = \frac{\langle p_x \rangle}{p_{total}} = \frac{1}{\beta\gamma}\frac{\sqrt{\langle v_x^2 \rangle}}{c} \tag{13}$$

The normalized, rms thermal emittance is then

$$\epsilon_N = \sigma_x \frac{\sqrt{\langle v_x^2 \rangle}}{c} \tag{14}$$

The mean squared transverse velocity for a Maxwell velocity distribution is,

$$\langle v_x^2 \rangle = \frac{\int_0^\infty v_x^2 e^{-\frac{mv_x^2}{2k_BT}} dv_x}{\int_0^\infty e^{-\frac{mv_x^2}{2k_BT}} dv_x} = \frac{k_BT}{m} \tag{15}$$

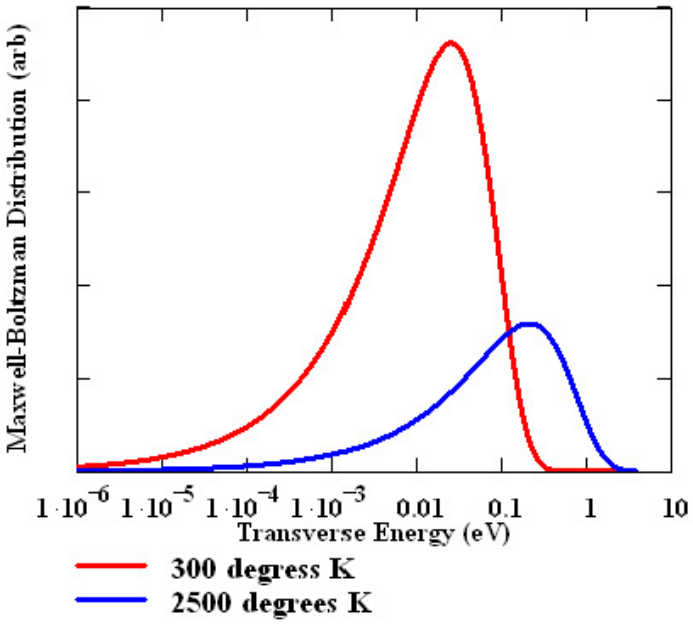

FIGURE 4. Maxwell-Boltzmann electron energy distributions at 300 degK where the rms electron energy spread is 0.049 eV, and at 2500 degK corresponding to an rms energy spread of 0.41 eV.

Therefore the thermionic emittance of a Maxwell-Boltzmann distribution at temperature, T, is

$$\epsilon_{thermionic} = \sigma_x \sqrt{\frac{k_B T}{mc^2}} \tag{16}$$

The divergence part of the cathode emittance contains all the physics of both the emission process and the cathode material properties and as such summarizes much of the interesting physics of the emission process. The beam size in coordinate space simply traces out the angular distribution to form the transverse phase space distribution as illustrated in Figure 5. Given that σ_x depends upon the particular transverse distribution being used, there is often a serious ambiguity which arises when expressing the thermal emittance in terms of "microns/mm". The confusion results in not knowing whether rms or flat top radii are used for the transverse radius. Therefore we suggest quoting a quantity called the normalized divergence, which for thermionic emission is

$$\Delta_{thermionic} \equiv \sqrt{\frac{k_B T}{mc^2}} \tag{17}$$

The thermal normalized divergence and the rms energy spread for the M-B distribution as a function of temperature is given in Figure 6.

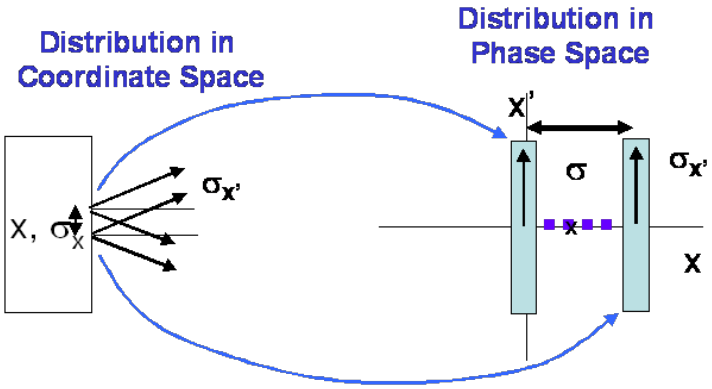

FIGURE 5. Each point on the cathode surface emits electrons according to the M-B velocity distribution, mapping into a 'line' of phase space points along the divergence axis. The emittance is then linear in the beam size with a divergence given by the M-B distribution at temperature T.

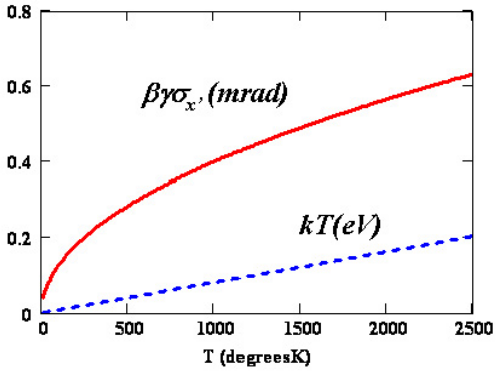

FIGURE 6. The normalized divergence and rms energy spread of the M-B gas as a function of temperature.

5. PHOTO-ELECTRIC EMISSION

Photoelectric emission from a metal can be described by the three steps of the Spicer model [Spicer]:

1. Photon absorption by the electron
2. Electron transport to the surface
3. Escape through the barrier

The kinematics of the first step is illustrated in Figure 7 showing the location of the vacuum state at the work function minus the Schottky energy. This Schottky energy accounts for the lower barrier when a large external field is applied to the cathode, and is typically a few ten's of an eV for fields of 100 MV/m. This schottky effect can significantly increase the quantum efficiency since the work function for a metal cathode like copper is 4.6 eV.

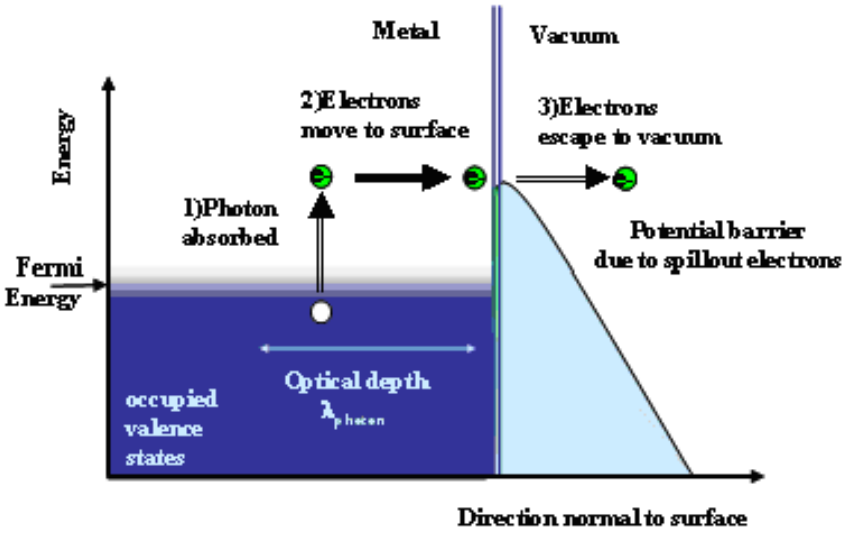

FIGURE 7. Spicer's three-step model of photoemission.

Some insight into the photo-emission process can be gained by assuming that all the electrons absorbing photons in step 1 escape. Then the quantum efficiency is simply proportional to the number of electrons the photon can excite above the barrier as indicated by the shaded region in the Figure 8. In addition the energy spread and hence the photo-electric emittance is also proportional to the photon energy. Therefore it appears that the higher the QE, the larger the photo-electric emittances. This is indeed true, as will be demonstrated below.

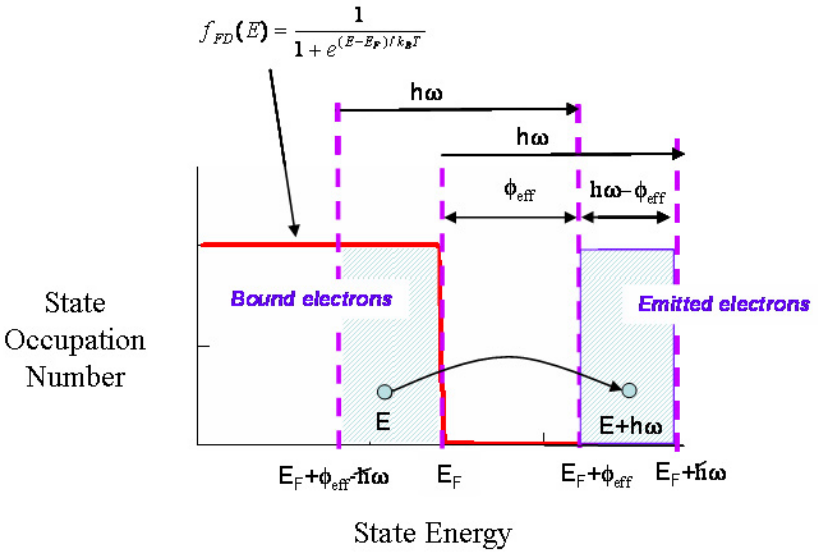

FIGURE 8. Kinematics of photo-emission.

During step 2, transport to the surface, the electron-electron scattering redistributes the energy distribution on a fast time scale, while the slower electron-phonon interaction acts on the electron through the lattice atoms. In general, the electron-phonon interaction is important for semi-conductor cathodes while electron-electron scattering is dominant for metals. These scattering interactions make step 2 a complex process with a time-dependence Fermi-Dirac temperature and a direct high-energy component. In one experiment, the time for the electrons to thermalize among themselves was measured in a laser pump-probe measurement [Fann et al., "Observation of the thermalization of electrons in a metal excited by femtosecond optical pulses," in Ultrafast Phenomenona, ed. J.-L. Martin, A. Meigus, G.A. Mourou and A.H. Zewail, Springer Verlag 1993, p331-334.]. Here the photoemission energy spectra were measured as a function of time delay between an IR pump laser and a UV probe. The electrons absorbed energy from the IR pulse, and having too low an energy to escape could only scatter and thermalize with other electrons and phonons. The UV probe sampled the electron energy distribution as a function of time by photo-emitting the electrons excited by the IR pulse. Fann's results are reproduced in Figure 9 and illustrate how the Step 1, high-energy electrons thermalize their energy on a time scale of approximately 400 fs, achieving a maximum Fermi-Dirac temperature of 700 degK. This experiment not only determined the electron-electron relaxation time, but also gives the thermodynamic parameters for the electronic equation-of-state.

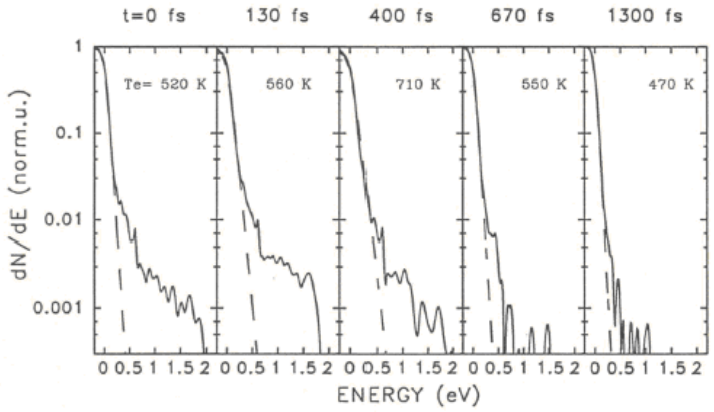

Fig. 1: Electron energy distribution function vs. energy with 120 μJ/cm^2 absorbed laser fluence at 5 time delays. The dashed line is the best Fermi-Dirac fit and the corresponding electron temperature, T_e, is shown. The vertical scale is in units of density of states.

FIGURE 9. Electron photo-emission spectra on the sub-ps time scale for Au.

Not only does the electron need to have enough energy to escape, but is must also be traveling toward the cathode surface. Therefore, the electron's momentum perpendicular to the surface, p_z, needs to satisfy,

$$\frac{p_z^2}{2m} > E_{Fermi} + \phi_{work} - \phi_{Schottky} \tag{18}$$

The longitudinal momentum is $p_z = p_{tot}cos\theta = \sqrt{2m(E+\hbar\omega)}cos\theta$, therefore the maximum angle of emission, max, satisfying the above condition is

$$cos\theta_{max} = \sqrt{\frac{E_F + \phi_{work} - \phi_{Schottky}}{E + \hbar\omega}} \tag{19}$$

where E_F is the cathode Fermi energy, ϕ_{work} is the work function for electron emission, $\phi_{Schottky}$ is the reduction in the barrier potential due to the external field, E is the electron's initial energy inside the cathode and is the photon energy. The relations between energy, momenta and angles at the surface are given in Figure 10. It's relevant to note that these momenta are for electrons just inside the cathode. The momenta outside the metal are discussed in a later section.

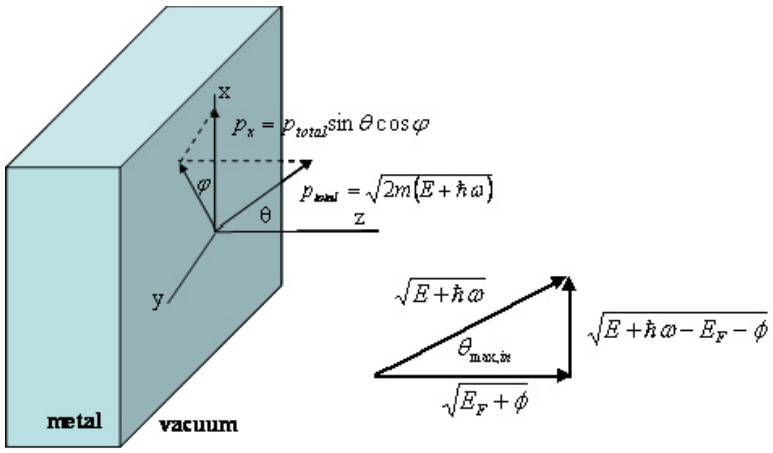

FIGURE 10. Definition of the maximum angle of emission for electrons at the cathode-vacuum boundary.

While the electron moves toward the surface, it can scatter with other electrons or with the lattice and excite phonons, lose energy and not escape the cathode. In a metal cathode, electron-electron scattering has a larger cross section than electron-phonon scattering. The mean free path for fermi gas of electrons can be computed by realizing that the Pauli principle leads to blocking of final states the electron scatter to and an relatively slow energy dependence of $(E-E_F)^{-3/2}$ near the Fermi energy [W. F. Krolikowski and W. E. Spicer, Phys. Rev. 185, 1969, 882-900]. The mean free path for electrons excited 4 to 5 eV above the Fermi energy is 45 to 70 angstroms. Since the absorption depth for a UV photon in copper is approximately 120 angstroms, the electrons absorbing photons at the greatest depth can on average scatter two to three times before reaching the surface. After one scattering, the electron loses too much energy to escape.

Putting all these elements together, the following expression for the QE is found [D. H. Dowell, K.K. King, R.E Kirby and J.F. Schmerge, "In situ cleaning of metal cathodes using a hydrogen beam," PRST-AB 9, 063502 (2006)] where $\phi_{eff} = \phi_{work} - \phi_{Schottky}$,

$$QE(\omega) = (1 - R(\omega))\frac{\int_{E_F+\phi_{eff}-\hbar\omega}^{E_F} F(E)dE \int_{\sqrt{\frac{E_F+\phi_{eff}}{E+\hbar\omega}}}^{1} d(cos\theta) \int_0^{2\pi} d\varphi}{\int dE \int d(cos\theta) \int d\varphi} \tag{20}$$

After some mathematics one finds,

$$QE(\omega) = \frac{(1 - R(\omega))}{1 + \frac{\lambda_{opt}}{\lambda_{e-e}}} \frac{E_F + \hbar\omega}{2\hbar\omega} \left(1 - \sqrt{\frac{E_F + \phi_{eff}}{E_F + \hbar\omega}}\right)^2 \tag{21}$$

Where $R(\omega)$ is the reflectivity, λ_{opt} is the photon's optical depth and λ_{e-e} is the electron mean free path.

The normalized divergence can be written in terms of the mean square of the transverse momentum which in turn is related to the electron distribution function, $g(E, \theta, \varphi)$, just inside the cathode surface,

$$\langle p_x^2 \rangle = \frac{\int\int\int g(E,\theta,\varphi) p_x^2 dE d(cos\theta) d\varphi}{\int\int\int g(E,\theta,\varphi) dE d(cos\theta) d\varphi} \tag{22}$$

The g-function and the integration limits depend upon the emission processes. For the three-step photo-emission model, g depends only on energy,

$$g_{photo} = (1 - f_{FD}(E + \hbar\omega)) f_{FD}(E) \tag{23}$$

Which is the mathematical expression for the electron distribution just below the Fermi energy shown as shaded in Figure 8. Since the Fermi-Dirac function, f_{FD}, at temperatures near ambient is well-represented by a Heaviside-step function which determines the limits on the energy integration. The θ-integration ranges from zero to θ_{max}, as given by Equation 25. Thus the mean square of the x-momentum defined in Figure 10, $p_x = \sqrt{2m(E + \hbar\omega)} sin\theta cos\varphi$, becomes

$$\langle p_x^2 \rangle = \frac{2m \int_{E_F + \phi_{eff} - \hbar\omega}^{E_F} dE \int_{\sqrt{\frac{E_F + \phi_{eff}}{E + \hbar\omega}}}^{1} d(cos\theta) \int_0^{2\pi} d\varphi (E + \hbar\omega) sin^2\theta cos^2\varphi}{\int dE \int d(cos\theta) \int d\varphi} \tag{24}$$

Performing these integrals results a relatively simple relation for the photo-electric normalized divergence,

$$\Delta_{photo} = \beta\gamma\sigma_{x'}^{photo} = \sqrt{\frac{\hbar\omega - \phi_{eff}}{3mc^2}} \tag{25}$$

The normalized divergence vs. photon energy for photo-electric emission is plotted in Figure 11 with 0, 50 and 100 MV/m applied fields. And the normalized cathode emittance for photo-emission is simply,

$$\epsilon_{photo} = \sigma_x \sqrt{\frac{\hbar\omega - \phi_{eff}}{3mc^2}} \tag{26}$$

Plotting these expressions for the emittance and the quantum efficiency in Figure 12 illustrates the strong correspondence between them as described above. A typical laser wavelength for copper cathodes is 255 nm, where the QE given by Equation 25 is 1.9×10^{-4} and 0.30 microns/mm for the emittance. The QE in an operating RF photocathode gun is nearly ten times lower(3×10^{-5}) and the measured emittance is 0.6 microns/mm.

Thus far the discussion of photoelectric emission has assumed the free electron gas model which is appropriate for metals. However emission from semi-conductor cathodes is distinctly different, and their treatment is beyond the scope of this lecture. An in depth discussion of this and other emission phenomena can be found in the recent book: Advances in Imaging and Electron Physics, Electron Emission Physics, Vol. 149, by K.L. Jensen.

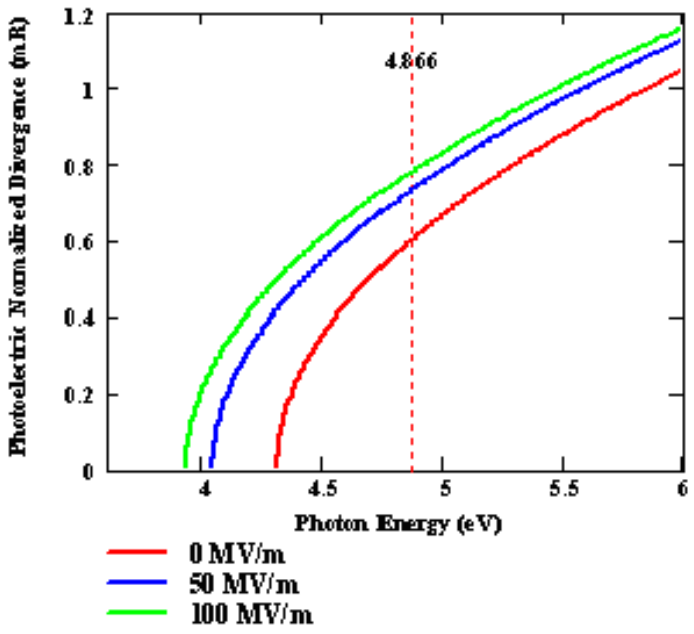

FIGURE 11. The normalized divergence plotted as a function of the photon energy for applied fields of 0, 50 and 100 MV/m. The 4.86 eV laser energy used for LCLS is shown by the vertical dash-line.

6. Field Emission

Field emission occurs under the influence of very high fields of 10^9 V/m or more. Since the electrons quantum mechanically tunnel through the barrier, the high electric fields are necessary to lower the barrier enough the achieve useful emission currents.

Field emission at electron temperatures above 1000 degK is referred to as thermal-field emission . This type of emission is used in thermionic rf guns which are commonly used as injectors for 3rd generation storage ring light sources. The effect of temperature is greatest at low fields and high temperatures (+1000 degK and higher) with the current density increasing by more than an order of magnitude over that at ambient (∼300 degK) temperature.

The field emission current density is given by

$$j_{field} = \int n(E_x, T) D(E_x, E_0) dE_x \tag{27}$$

where the supply function, $n(E_x, T)$, is the flux of electrons incident upon the barrier with energies between E_x and $E_x + dE_x$. The barrier as shown in Figure 2 is determined by the work function, the image charge and the applied electric field, E_0. The transmission of electrons through this barrier is given by the transparency function, $D(E_x, E_0)$. This function can be solved using the WKB approximation

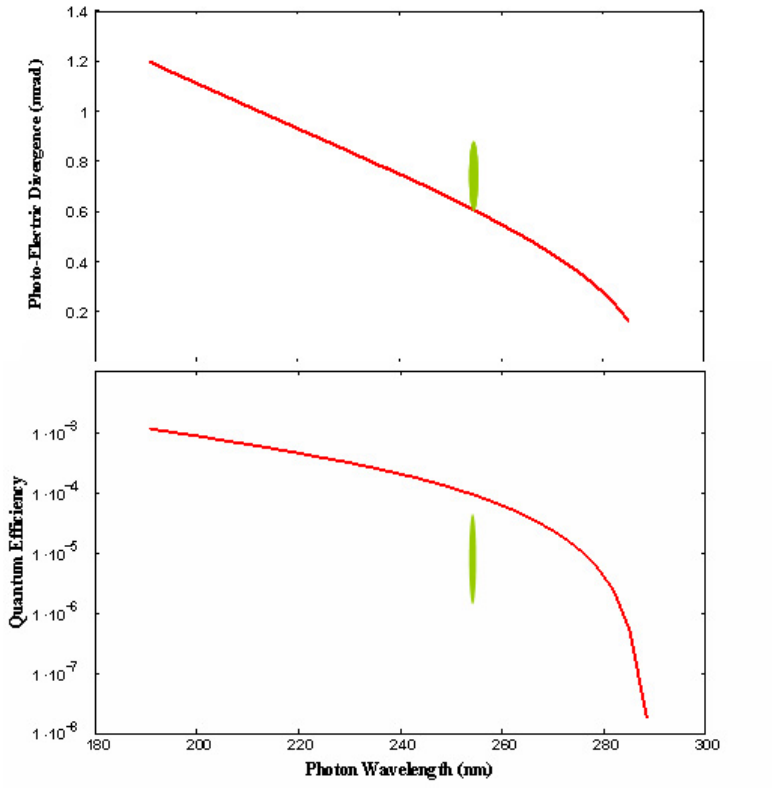

FIGURE 12. The photo-electric normalized divergence (top, red) and the quantum efficiency (bottom, red) vs. photon wavelength for copper. The green ellipses show the range of QE and cathode emittance measured during commissioning of the LCLS injector.

for a barrier produced by the image charge and the applied field,

$$\phi_{Schottky}(x) = -\frac{e^2}{16\pi\epsilon_0 x} - eE_0 x \tag{28}$$

The resulting transparency function is

$$D(E_x, E_0) = \exp\left[\frac{-8\pi\sqrt{2m}}{3he}\frac{E_x^{3/2}}{E_0}\theta\left(\frac{\sqrt{e^3E_0}}{\phi_{work}}\right)\right] \tag{29}$$

where $\theta(y)$ is the Nordheim function (not to be confused with the angle, θ). Although the θ -function is strongly dependent upon y and is mathematically complicated, it monotonically varies from 1 to 0 on the interval $0 < y < 1$ and to a very good approximation can be represented by

$$\theta(y) = 1 - 0.142y - 0.855y^2 \tag{30}$$

The supply function for a Fermi-Dirac electron gas was also derived by Nordheim,

$$n(E_x, T) = \frac{4\pi m k_B T}{h^3}\ln\left(1 + e^{\frac{E_x - E_F}{k_B T}}\right) \tag{31}$$

Combining the supply and transparency functions the electron energy spectrum is simply,

$$N_{field}(E_x, E_0, T) = n(E_x, T)D(E_x, E_0) \tag{32}$$

The combination of these three functions is plotted in Figure 13 vs. the electron energy.

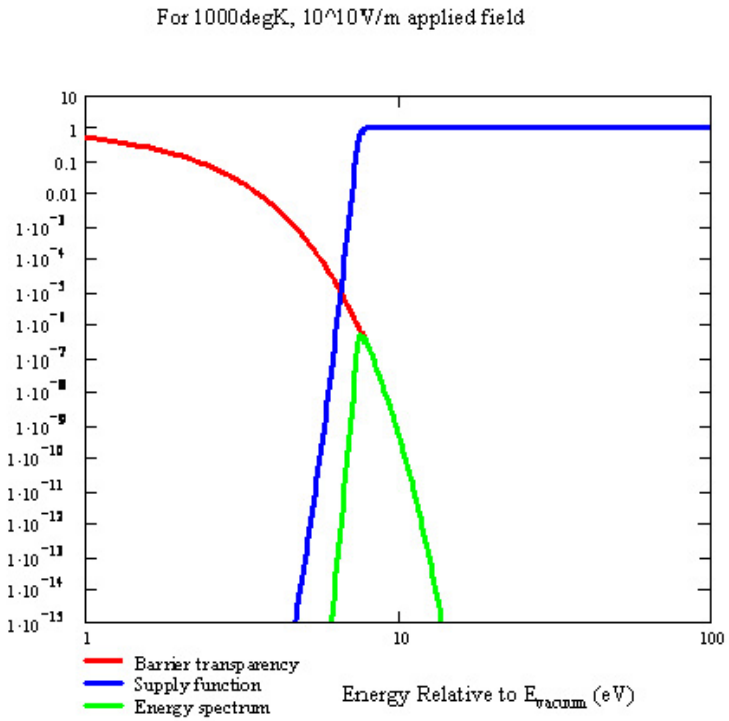

FIGURE 13. The spectrum of the emitted electrons results from the overlap of the barrier transparency (blue) with the supply function (red). In this case, the supply function is for a Fermi-Dirac distribution at a temperature of 300 degK .

In field emission the electron yield is exponentially sensitive to the external field and any significant current requires fields in excess of 10^9 V/m as seen in Figure 14. Such high fields are achieved by using pulsed high voltages and/or field-enhancing, sharp emitters. Knowledge of the energy spectra allows numerical computation of the rms energy spread and the field emission emittance which are plotted in Figure 15 for external fields between 10^9 and 10^{10} Volts/m.

7. Discussion of the Three Emission Processes

The last three sections derived the cathode emittances for the three emission processes: thermionic, photo-electric and field emission. Rather than using the term, thermal emittance, we prefer to using cathode emittance for the emission processes. And to specifically derive the cathode emittance for each of the three

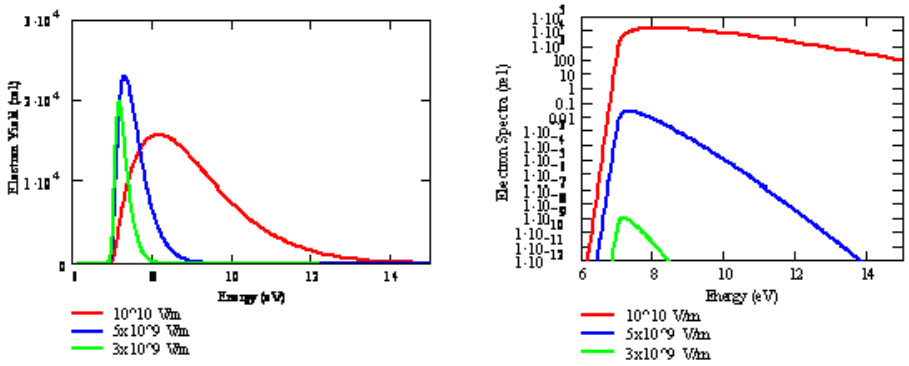

FIGURE 14. Electron spectra for field emission electrons for various applied fields. Left: Electron emission spectra plotted with a linear vertical scale and with arbitrarily normalization to illustrate the spectral shapes. Right: The spectral yields plotted logarithmically to illustrate the strong dependence of yield and shape upon applied field.

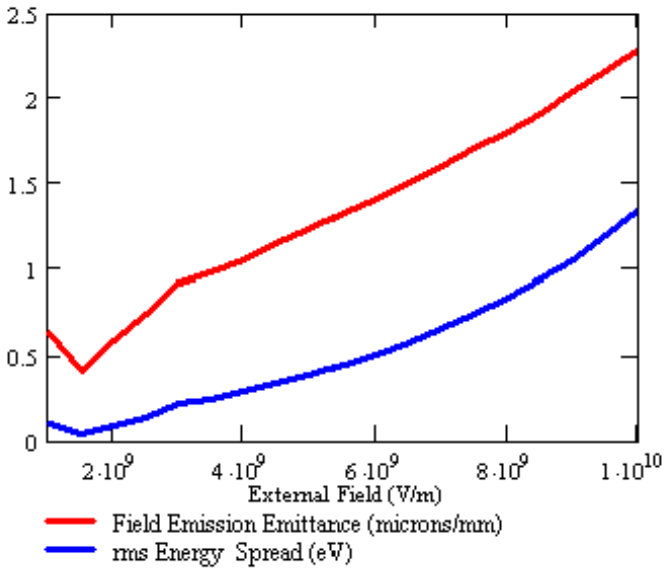

FIGURE 15. The energy spread and field emission emittance from a planar emitter as functions of the external field.

emission processes. The cathode emittance for thermionic emission is approximately 0.3 microns/mm for a cathode temperature of 2500 degK. The photoelectric emittance ranges between 0.5 to 1 micron/mm depending upon the photon wavelength and was shown to be proportional to the quantum efficiency. The

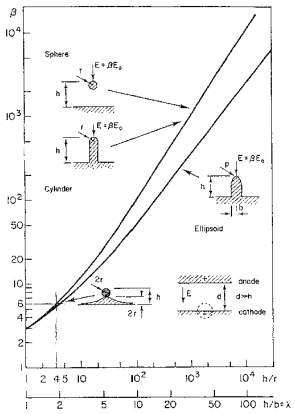

Fig 4.4 A collated representation of the field enhancement factors β associated with various idealised microprotrusion geometries. (From Rohrbach [31], with permission.)

FIGURE 16. Field enhancement factors for various shapes.

field-emission emittance varies from 0.5 to 2 microns/mm for fields corresponding to fields of 10^9 to 10^{10} V/m, and hence has larger emittance for the same source size than the other two processes. In many cases electron guns combine field emission with the other two processes to produce electrons. A good example is photo-electric emission in a high field gun, where field-emission lowers the barrier height via the Schottky effect and increases the quantum efficiency.

8. The Refraction of Electrons at the Cathode Surface

Similar to photons, electrons change their angle or refract as they transit the cathode surface. This is a result of the boundary condition requiring conservation of the transverse momentum across the cathode-vacuum interface. Using the momenta and angles defined in Figure 17, the boundary condition is expressed as

$$p_x^{in} = p_x^{out} \tag{33}$$

$$p_x^{in} = p_{total}^{in} sin\theta_{in} = p_{total}^{out} sin\theta_{out} = p_x^{out} \tag{34}$$

The total energy of the electron inside the cathode after absorbing the photon is $E + \hbar\omega$. Thus the total momentum inside is,

$$p_{total}^{in} = \sqrt{2m(E + \hbar\omega)} \tag{35}$$

and outside the total momentum is

$$p_{total}^{in} = \sqrt{2m(E + \hbar\omega - E_F - \phi_{eff})} \tag{36}$$

Inserting these expressions into Equation 34 and solving for the ratio of sines gives a formula similar to Snell's law,

$$\frac{sin\theta_{out}}{sin\theta_{in}} = \sqrt{\frac{E + \hbar\omega}{E + \hbar\omega - E_F - \phi_{eff}}} \tag{37}$$

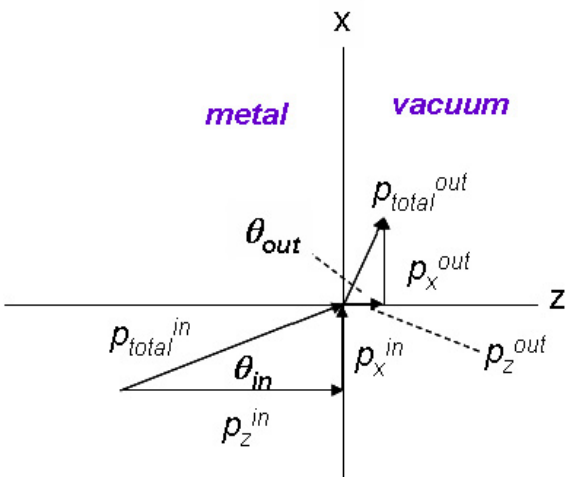

FIGURE 17. Definitions of the electron momenta and angles at the boundary between the cathode and vacuum.

An electron approaching the boundary needs to have sufficient momentum to overcome the barrier,

$$p_z = \sqrt{2m(E+\hbar\omega)}cos\theta_{in} \geq \sqrt{2m(E_F+\phi_{eff})} \tag{38}$$

This leads to the maximum escape angle, θ_{in}^{max},

$$cos\theta_{in}^{max} = \sqrt{\frac{E_F+\phi_{eff}}{E+\hbar\omega}} \tag{39}$$

and

$$sin\theta_{in}^{max} = \sqrt{\frac{E+\hbar\omega-E_F-\phi_{eff}}{E+\hbar\omega}} \tag{40}$$

these relations are shown graphically in Figure 18.

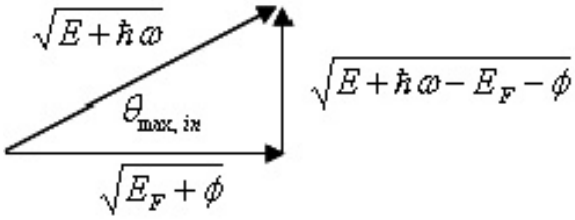

FIGURE 18. Graphical relation between electron, Fermi and work function energies.

On the vacuum side of the boundary the maximum electron angle is,

$$sin\theta_{out}^{max} = sin\theta_{in}^{max}\sqrt{\frac{E+\hbar\omega}{E+\hbar\omega-E_F-\phi_{eff}}} \longrightarrow \theta_{out}^{max} = \pi/2 \tag{41}$$

and the electron behaves just like a photon and undergoes total internal reflection for angles greater than the the critical angle, θ_{in}^{max}.

Thus it is reasonable to associate the square root of these energies with the following indices of refraction for the electron inside and outside the cathode, respectively,

$$n_{in} = \sqrt{E + \hbar\omega} \tag{42}$$

$$n_{out} = \sqrt{E + \hbar\omega - E_F - \phi_{eff}} \tag{43}$$

This analogy suggests focusing effects for the escaping electrons, as discussed in the next section.

9. Focusing of Electrons by the Cathode-Vacuum Boundary

The bending of light by a curved boundary between media with different indices of refraction is illustrated in Figure 19 and expressed as (see for example, "Optics," by Miles V. Klein, John Wiley & Sons, Inc, 1970, pp. 67-69),

$$x_1 = \left[\frac{(n_0 - n_1)D_1}{n_1 R} + 1\right] x_0 + \left[D_0 + \frac{n_0 D_1}{n_1} + \frac{(n_0 - n_1)D_0 D_1}{n_1 R}\right] \theta_0 \tag{44}$$

$$\theta_1 = \frac{n_0 - n_1}{n_0 R} x_0 + \left[\frac{n_0}{-n_1} + \frac{(n_0 - n_1)D_0}{n_1 R}\right] \theta_0 \tag{45}$$

In comparison with the paraxial equations for ray-optics, the focal strength of the refracting boundary is,

$$\frac{1}{f} = \frac{n_1 - n_0}{n_1 R} \tag{46}$$

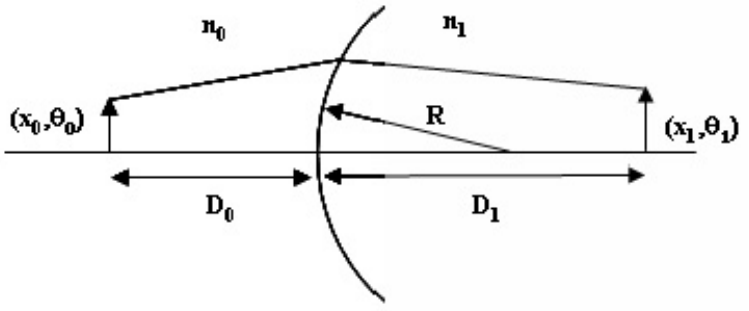

Figure 19. Quantities used in the relations for refraction at and indexed boundary

Inserting the previously derived relations for the electron indices of refraction gives,

$$\frac{1}{f} = \frac{1}{R}\left[1 - \sqrt{\frac{E+\hbar\omega}{E+\hbar\omega-(E_F+\phi_{eff})}}\right] \tag{47}$$

Clearly the square root term is always greater than unity, making the quantity in the brackets negative. Therefore surfaces with positive curvature will give the electrons a diverging angle, while negative curvature surfaces give them a converging angle.

Since the electrons are all emitted from a thin layer an optical depth thick, then $D_0 \approx 0$ and Equations 44 and 45 become,

$$x_1 = \left[\frac{(n_0-n_1)D_1}{n_1 R}+1\right]x_0 + \frac{n_0 D_1}{n_1}\theta_0 \tag{48}$$

$$\theta_1 = \frac{n_0-n_1}{n_0 R}x_0 - \frac{n_0}{n_1}\theta_0 \tag{49}$$

10. The Debye Length and Laminar Flow

Once free of the cathode, the electrons experience both external and internal mutual forces. The external forces are those imposed by RF, magnetic and electric fields. These are forces which the designer of the injectors can use to create and control the beam. The internal forces results from the mutual interactions between the electrons, which can be classified into collisions and smoothly varying forces. The collisional forces occur between nearest neighbors and are random, statistical fluctuations related to the beam temperature. On a larger scale lengths the electrons will collectively move to screen any non-uniform of the electron distribution, resulting in a slowly, varying spatial field. This screening of the single-particle forces is called Debye shielding [Reiser, p 184; Jackson, 1st Edition, pp 339] and is effective for distances greater than the Debye length, λ_D, which is defined as the ratio of the beam's random, thermal velocity to the plasma frequency, $\omega_p = \sqrt{\frac{e^2 n}{\epsilon_0 m}}$, where n is the electron density and m is the electron mass,

$$\lambda_D = \frac{\sqrt{\langle v_x^2\rangle}}{\omega_p} \tag{50}$$

Assuming M-B statistics, the Debye length in the beam rest frame is

$$\lambda_D = \sqrt{\frac{\epsilon_0 k_B T_b}{e^2 n}} \tag{51}$$

The procedure for the relativistic transformation of this relation to the lab frame is ambiguous as described by Reiser who simply uses $T = T_b/\gamma$ to obtain the laboratory frame Debye length in terms of laboratory quantities, n, γ and the beam rest frame temperature, T_b,

$$\lambda_D = \sqrt{\frac{\epsilon_0 \gamma k_B T_b}{e^2 n}} \tag{52}$$

In some cases, and especially when the electrons have just escaped from the cathode, the electron statistics are not necessarily given by the M-B thermal distribution.

On length scales where the Debye length is large compared to the distance between the electrons and comparable to the beam size, the collective space charge

interactions are diminished and independent particle dynamics dominate. As an example consider the 135 MeV, 1 nC beam in the LCLS injector with a radius of 100 microns and a bunch length of 6 ps and a thermal temperature $k_B T_b$ of 0.2 eV, for which λ_D is 5.1 microns. The inter-particle distance is 0.2 microns. Since the Debye length determines the shortest plasma wavelength, in this case, beam plasma waves shorter than 5 microns are not possible. The shorter wavelength oscillations are washed out by the thermal motion of the electrons. When the space charge wave velocity is close to the thermal velocity and the waves are Landau damped. (Jackson, 1st Edition, pp340.)

11. The Space Charge Limit and Cathode Emittance

In this section it is shown that space charge limited emission for a cathode emitting a short electron bunch evolves toward the Child-Langmuir law as the bunch length increases and the region between the bunch and cathode becomes filled with electrons. A general expression for the space charge limit is derived first for a short bunch near the cathode surface and then for a continuous current of electrons streaming from the cathode, yielding the Child-Langmuir law without having to solve Poisson's second-order differential equation. This result is used to compute the emittance for photo-electric emission at the space charge limit.

Consider the electron bunch of length δ when it is a short distance d from the cathode surface as shown in Figure 1. If d is small compared to the beam's transverse dimension, then Gauss's law is trivially integrated over the cylinder's surface to solve for the space charge electric field between the cathode and a thin sheet of electrons.

$$\oint_S \vec{\mathbf{E}} \cdot \vec{\mathbf{n}} dS = \frac{1}{\epsilon_0} \int_V \rho(\vec{r}) d^{\,3}\boldsymbol{r} \tag{53}$$

And obtain the space charge field of a sheet beam,

$$E_z = \frac{\sigma}{\epsilon_0} \tag{54}$$

We reach the space charge limit (SCL) when the space charge field, E_z equals the applied, external field, E_a. That is,

$$\sigma_{SCL} \equiv \epsilon_0 E_a \tag{55}$$

The space charge potential energy of the short bunch is obtained by a simple integration along z,

$$\frac{d\phi}{dz} = E_z = \frac{\sigma}{\epsilon_0} \tag{56}$$

Thus the surface charge density corresponding to the SCL in terms of the potential energy is given by,

$$\sigma_{SCL} = \frac{\epsilon_0 \phi_a}{d} \tag{57}$$

Next we derive the Child-Langmuir law, and begin by expressing the beam current density in terms of the charge density and beam velocity, βc,

$$J = \rho \beta c = \frac{\sigma}{\delta} \beta c \tag{58}$$

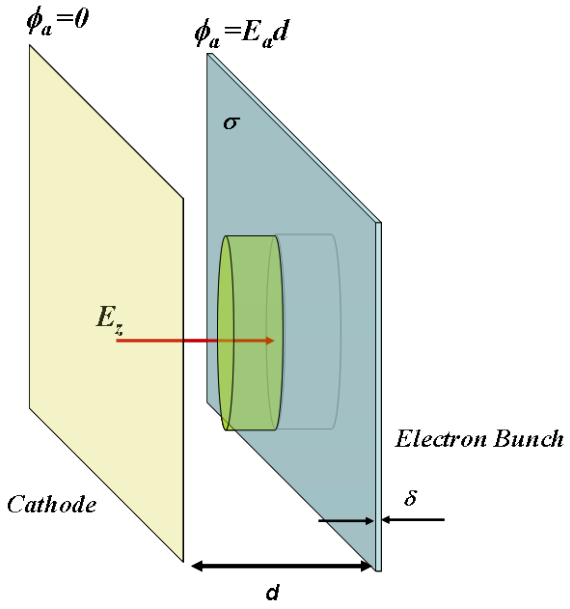

FIGURE 20. The cathode and electron bunch shortly after emission. The electron bunch is typically 10's of microns long when the laser pulse ends and the last electron is emitted. d is the distance from the cathode to the tail of a bunch which is δ long.

We assume the electrons have negligible initial velocity at the cathode surface, and thus their kinetic energy equals the applied potential, $\beta c = \sqrt{\frac{2e\phi_a}{m}}$. This gives the SCL peak current density of the short bunch as,

$$J_{SCL}^{bunch} = \epsilon_0 \sqrt{\frac{2e}{m}} \frac{\phi_a^{3/2}}{\delta d} \tag{59}$$

When the electrons fill the region between the cathode and the head of the bunch, $\delta = d$,

$$J_{SCL}^{CL} = \epsilon_0 \sqrt{\frac{2e}{m}} \frac{\phi_a^{3/2}}{d^2} \tag{60}$$

which except for the missing factor of 4/9 (see Reiser p. 46) is the well-known Child-Langmuir law for current flowing in a diode region.

The space charge limited emittance is found by combining the beam size for a the short bunch at the SCL with the normalized divergence derived for photo-electric emission. If we assume the beam is transversely unform with radius a then

$$a = \sqrt{\frac{Q_{bunch}}{\epsilon_0 \pi E_a}} \tag{61}$$

Which has the root-mean-square size of

$$\sigma_x = \frac{a}{2} = \sqrt{\frac{Q_{bunch}}{4\pi\epsilon_0 E_a}} \tag{62}$$

The normalized cathode emittance is given by

$$\varepsilon = \beta\gamma\sigma_x\sigma_{x'} \tag{63}$$

And substituting the normalized divergence for photo-electric emission results in the SCL photo-electric emittance,

$$\varepsilon_{photo}^{SCL} = \sqrt{\frac{Q_{bunch}(\hbar\omega - \phi_{eff})}{4\pi\epsilon_0 mc^2 E_a}} \tag{64}$$

Here ϕ_{eff} is the effective cathode work function which includes the Schottky effect and $\hbar\omega$ is the laser photon energy. For a bunch charge of 1 nC, an applied field of 50 MV/m, a laser energy of 4.86 eV and a copper cathode ($\phi_{eff} = 4.5eV$), the space charge limited thermal emittance is

$$\varepsilon_{photo}^{SCL} = 0.34\ microns \tag{65}$$

12. Charge Limited Emission in RF Guns

When a transverse gaussian beam reaches the short bunch space charge limit, emission saturates and the charge becomes constant and independent of the laser energy. This constant charge is over an area defined by Eqn. 61,and results in the charge vs the drive laser energy shown in Figures 21 and 22. The charge at low laser energy depends linearly on the laser energy while at high laser energy the charge rolls over due to the space charge limit. A larger laser size reduces the space charge field and gives more charge for the same laser energy. The linear region QE limits the emission, while space charge limited emission occurs at the high laser fluence as illustrated experimentally in the figures.

13. The Envelope Equation and Beam Perveance

The envelope equation without external focusing is,

$$r_m'' = \frac{\epsilon^2}{r_m^3} + \frac{K}{r_m} \tag{66}$$

where K is the generalized perveance (Lawson, p117) and ϵ is the geometric emittance,

$$K_{general} = \frac{I}{I_0}\frac{2}{\beta^3\gamma^3} = \frac{\omega_p^2 a^2}{2\beta^2 c^2}. \tag{67}$$

Otherwise the perveance is defined as (Reiser, Eqn. 4.28, p.197)

$$K = \frac{I}{4\pi\epsilon_0 V^{3/2}\left(\frac{2e}{m}\right)^{1/2}} = \frac{I}{d^2 J_{SCL}^{CL}} \tag{68}$$

Where the denominator is identified as the Child-Langmiur current from Eqn. 60. Therefore the perveance is defined as the beam current divided by the space charge limited current, $d^2 J_{SCL}^{CL}$.

When the beam is in radial equilibrium, $r_e'' = 0$, the geometric emittance can be related to the perveance,

$$\frac{\epsilon^2}{r_e^3} = \frac{K}{r_e} \tag{69}$$

$$\epsilon = r_e\sqrt{K} \tag{70}$$

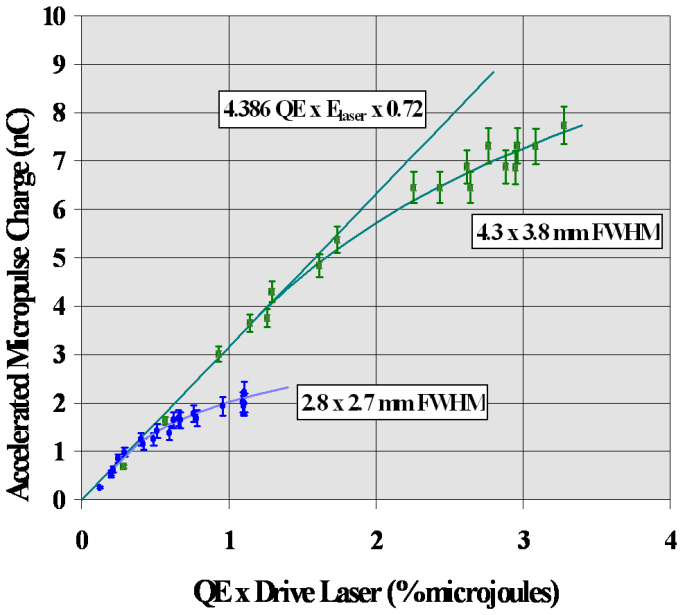

FIGURE 21. The charge vs. the drive laser energy for 433 MHz RF photocathode gun operating with a peak cathode field of 25 MV/m. The two sets of data are shown with curves corresponding to measured x and y laser sizes. The straight line gives the cathode QE. (Adamski et al., SPIE Vol. 2988, p158-169.)

$$\epsilon = r_e \sqrt{\frac{I}{V^{3/2}} \left[\frac{1}{4\pi\epsilon_0 \left(\frac{2e}{m}\right)^{1/2}} \right]} = r_e \sqrt{\frac{I}{d^2 J_{SCL}^{CL}}} = r_e \sqrt{K} \tag{71}$$

Thus the square root of the perveance is the space charge limited *geometric* divergence.

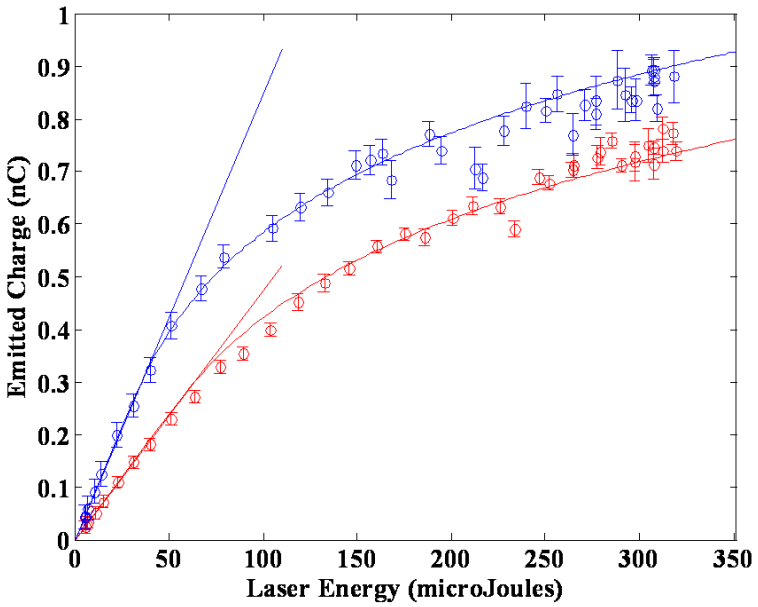

FIGURE 22. Measurements of the charge vs. the laser energy for the LCLS-gun operating at a peak cathode field of 115 MV/m. The data were taken with the same beam size (1.2 mm diameter) but for different QE.